Supplementary Material for

Deformation behavior and energy absorption capability of polymer and ceramic-polymer composite microlattices under cyclic loading

Almut Schroer[a)], Jeffrey M. Wheeler[b)], Ruth Schwaiger[a),*]
a) Institute for Applied Materials (IAM), Karlsruhe Institute of Technology (KIT), P.O. Box 3640, 76021 Karlsruhe, Germany
b) Department of Materials, ETHZ – Swiss Federal Institute of Technology, Vladimir-Prelog-Weg 5, 8093 Zurich, Switzerland
* Corresponding author. E-mail address: ruth.schwaiger@kit.edu (R. Schwaiger)

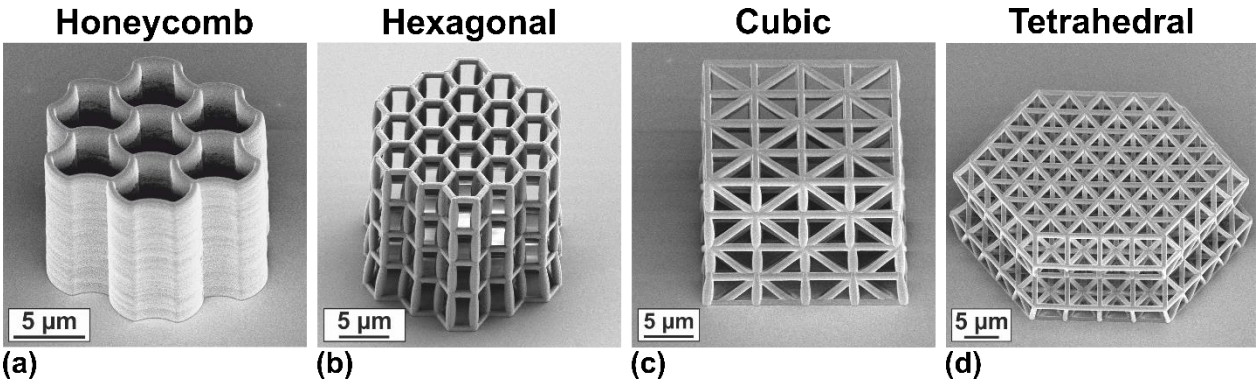

Figure S.1: SEM-images of microlattices with different types of architecture in the untested condition, a) honeycomb, b) hexagonal, c) cubic with fully diagonal bracings, d) tetrahedral structure. The strut length of the vertical struts within the hexagonal and the cubic structures as well as all strut lengths within the tetrahedral structures are kept constant, with a strut length of 5 µm.

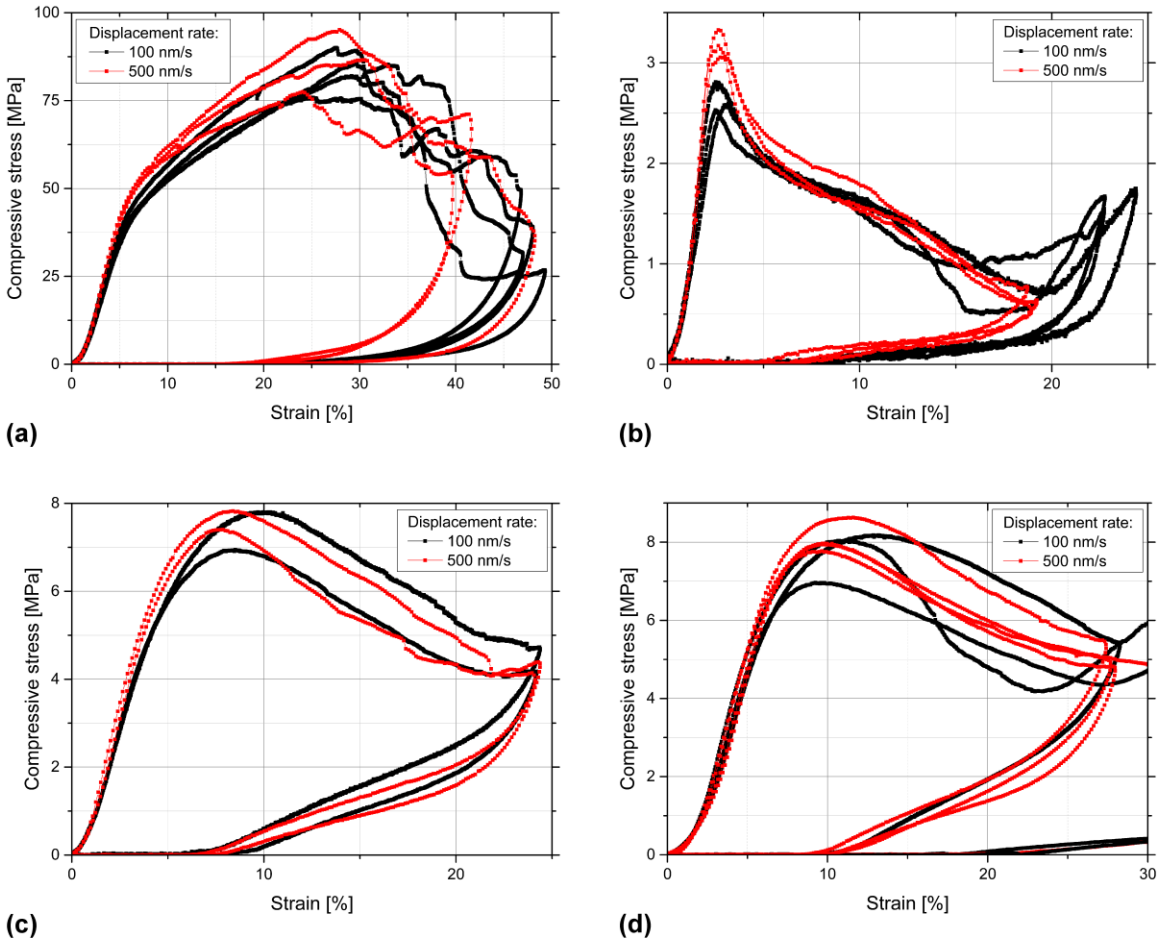

Figure S.2: Compressive stress-strain curves of as-written structures with different types of architecture, compressed at different displacement rates of 100 nm/s (black curves) and 500 nm/s (red curves). a) Honeycomb, b) hexagonal, c) cubic with fully diagonal bracings, d) tetrahedral structure.

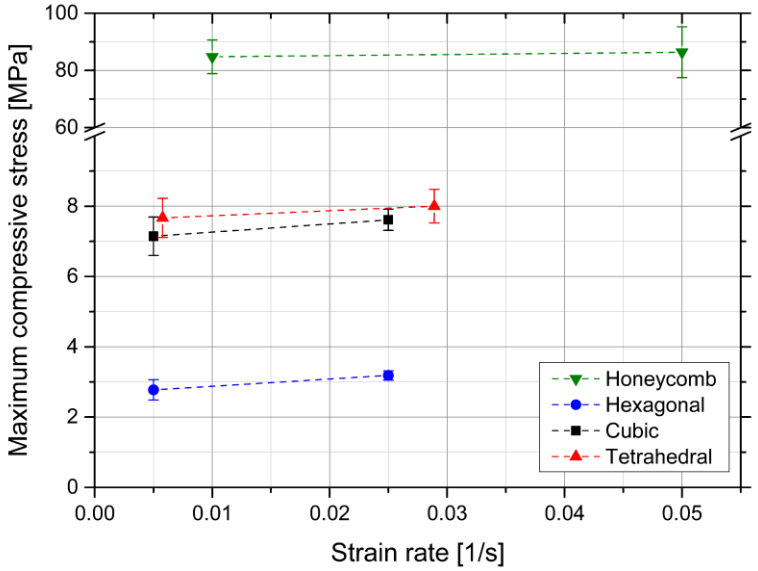

Figure S.3: Average maximum compressive stress values of as-written structures with different types of architecture as a function of the strain rate during compression testing. Error bars show the standard deviation of at least two tests.

Table S.1: Characteristics of energy dissipation of as-written structures: Both the specific dissipated energy and the remaining strain are normalized by the corresponding quantities of the first cycle. The decrease of the specific dissipated energy and the increase of the remaining strain is listed for cycle 2 and 20, and the loss coefficient for cycles 1, 2, and 20.

	Normalized specific dissipated energy		**Normalized remaining strain**		**Loss coefficient Ψ [-]**		
	$\Delta U_2/\Delta U_1$ [-]	$\Delta U_{20}/\Delta U_1$ [-]	$\Delta \varepsilon_2/\Delta \varepsilon_1$ [-]	$\Delta \varepsilon_{20}/\Delta \varepsilon_1$ [-]	**Cycle 1**	**Cycle 2**	**Cycle 20**
Honeycomb	0.16	0.02	1.21	1.80	0.93 ± 0.01	0.751 ± 0.002	0.54 ± 0.02
Hexagonal	0.25	0.05	1.22	2.30	0.85 ± 0.04	0.61 ± 0.02	0.40 ± 0.01
Cubic	0.33	0.08	1.12	1.62	0.82 ± 0.01	0.63 ± 0.01	0.42 ± 0.01
Tetrahedral	0.36	0.11	1.09	1.49	0.82 ± 0.01	0.66 ± 0.02	0.47 ± 0.02

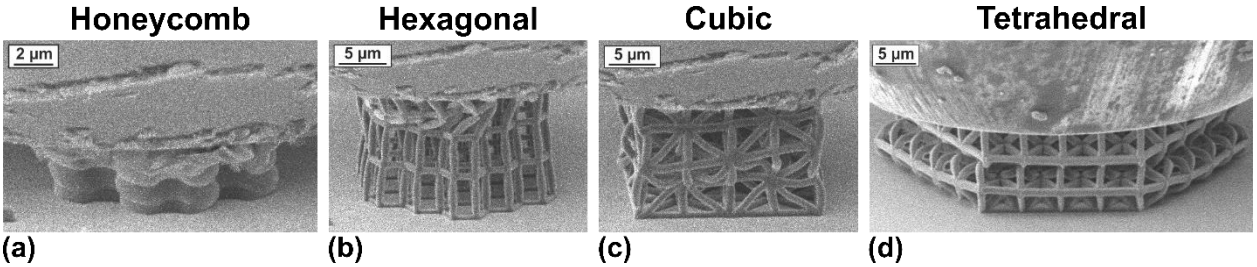

Figure S.4: Video frame stills from *in-situ* testing of as-written structures with different types of architecture, a) honeycomb, b) hexagonal, c) cubic with fully diagonal bracings, d) tetrahedral structure. The video frames show the structures at the maximum displacement of 5 µm during a first cycle of compression testing, thus, in the highest deformed state. For all structures local and global buckling is clearly visible. The hexagonal structure (b) shows the least even distributed deformation over the whole structure with already fracture nodes visible.

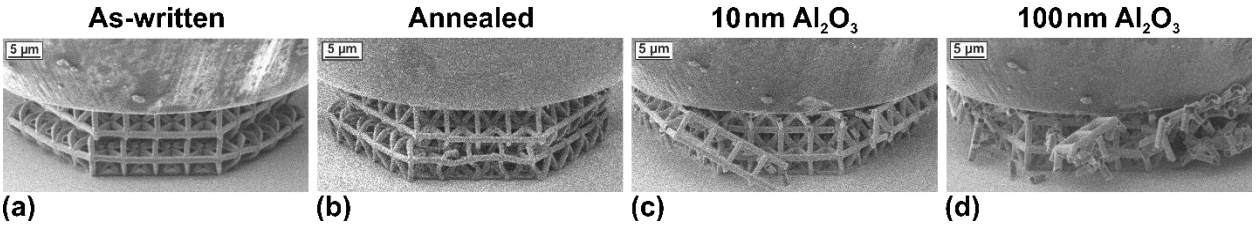

Figure S.5: Video frame stills from *in-situ* testing of tetrahedral structures with different processing conditions, a) as-written, b) annealed at 200°C for 15 min, c) with 10 nm Al_2O_3 coating, d) with 100 nm Al_2O_3 coating. The video frames show the structures at the maximum displacement of 5 µm during a first cycle of compression testing, thus, in the highest deformed state. For the polymeric samples (a, b) buckling of the ligaments is clearly visible whereas for the coated structures (c, d) the catastrophic fracture of the structures is obvious.

Table S.2: Characteristics of energy dissipation of tetrahedral structures, i.e. in the as-written state, annealed, with a 10 nm thick and a 100 nm thick alumina coating: Both the specific dissipated energy and the remaining strain are normalized by the corresponding quantities of the first cycle. The decrease of the specific dissipated energy and the increase of the remaining strain is listed for cycles 2 and 20, and the loss coefficient for cycles 1, 2, and 20.

		Normalized specific dissipated energy		Normalized remaining strain		Loss coefficient Ψ [-]		
		$\Delta U_2/\Delta U_1$ [-]	$\Delta U_{20}/\Delta U_1$ [-]	$\Delta\varepsilon_2/\Delta\varepsilon_1$ [-]	$\Delta\varepsilon_{20}/\Delta\varepsilon_1$ [-]	Cycle 1	Cycle 2	Cycle 20
As-written		0.363	0.106	1.09	1.49	0.82 ± 0.01	0.66 ± 0.02	0.47 ± 0.02
Annealed		0.372	0.103	1.20	2.51	0.77 ± 0.06	0.62 ± 0.03	0.47 ± 0.01
Alumina	**10 nm**	0.052	0.015	1.03	1.14	0.959 ± 0.002	0.60 ± 0.02	0.403 ± 0.002
	100nm	0.010	0.003	1.10	1.18	0.99 ± 0.01	0.47 ± 0.05	0.36 ± 0.05

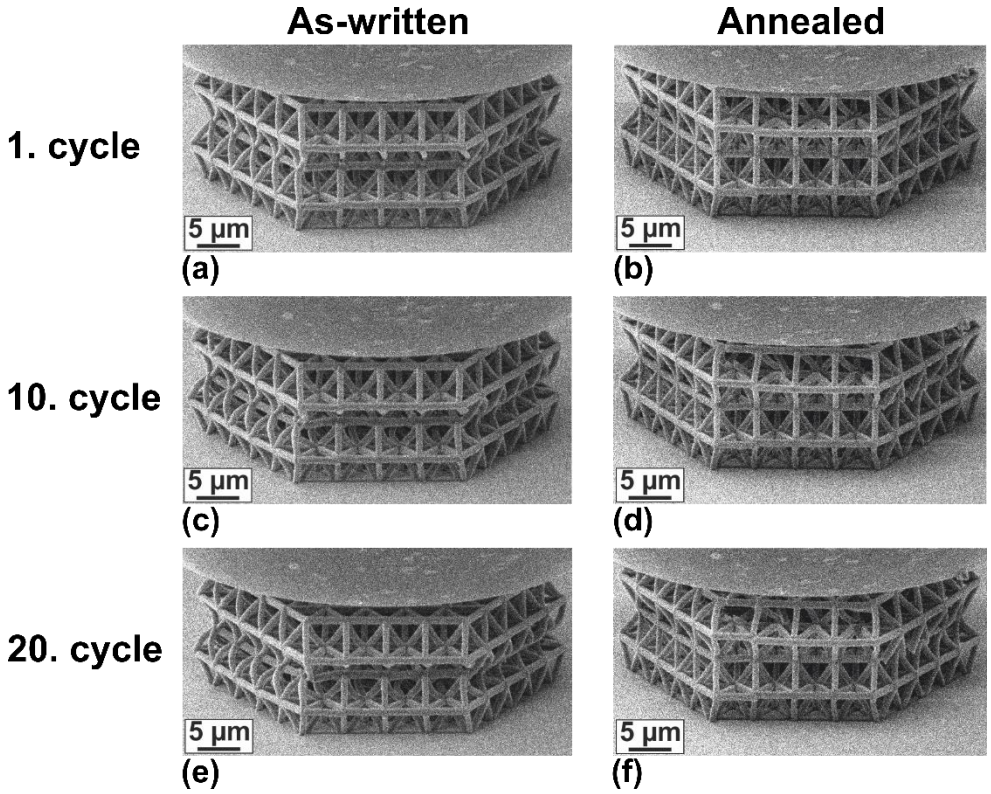

Figure S.6: Video frame stills from *in-situ* testing of tetrahedral structures with different processing conditions, a), c), e) as-written, b), d), f) annealed at 200°C for 15 min. The video frames show the structures after unloading of cycle 1 (a, b), cycle 10 (c, d) and cycle 20 (e, f). The higher remaining strain after unloading for the as-written sample is visible (compare Figure 7).

Table S.3: Specific dissipated energy during progressive cycling for tetrahedral structures. Three different deformation regimes were identified: regime 1 before the maximum stress was reached, regime 2 from the maximum stress to the cycle prior to localized compression, regime 3 covering the cycles with localized compression. In addition, the total specific dissipated energy as well as the corresponding cycle numbers N together with the fractions in the different regimes.

			Regime 1			Regime 2			Regime 3		
Specific dissipated energy		**Total [kJ/kg]**	**N**	**Sum [kJ/kg]**	**Fraction [%]**	**N**	**Sum [kJ/kg]**	**Fraction [%]**	**N**	**Sum [kJ/kg]**	**Fraction [%]**
As-written		12.3	1-3	0.5	4.3	4-9	9.8	79.7	10	2.0	16.0
Annealed		15.5	1-4	1.2	7.8	5-9	11.8	76.3	10	2.5	15.9
Alumina	**10 nm**	15.1	1-3	1.6	10.3	4-6	10.1	67.1	7-10	3.4	22.6
	100 nm	17.0	1-3	1.6	9.2	4-5	13.4	79.1	6-10	2.0	11.8

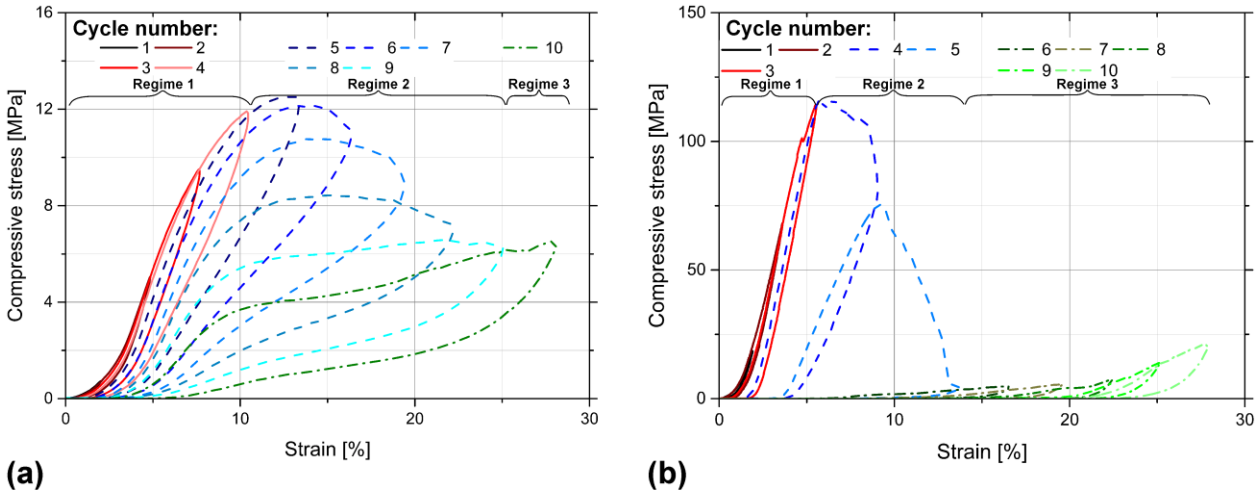

Figure S.7: Individual cycles of progressive loading of tetrahedral structures with different processing conditions, a) annealed at 200°C for 15 min, b) with 100 nm Al_2O_3 coating. The cycles before the maximum stress – Regime 1 – is reached are indicated by continuous red lines. The following cycles are marked with dashed blue lines – Regime 2 – until localized compression occurs. The cycles with localized compression – Regime 3 – are shown as dashed-dotted green lines.

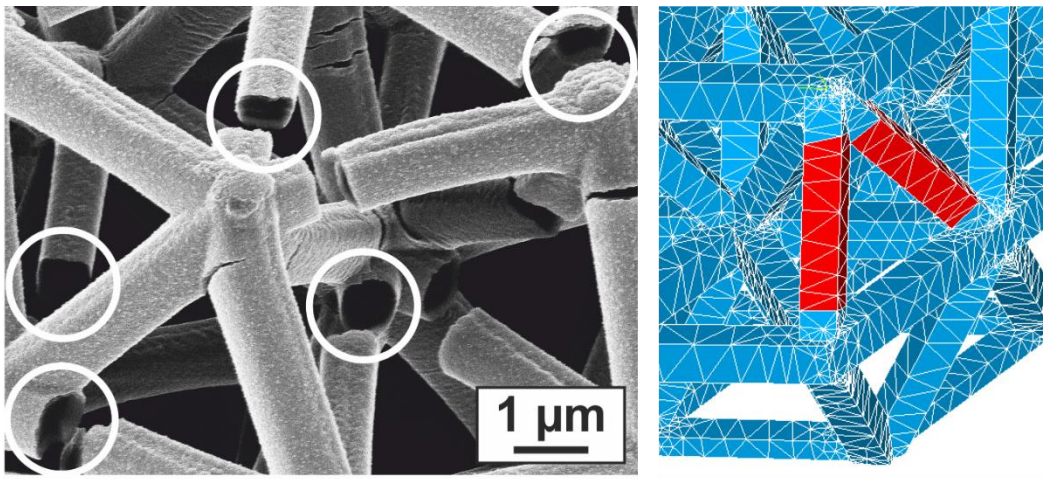

Figure S.8: a) HIM-image of fractured tetrahedral structure, to visualize the nature of the rectangular cross-sections of the ligaments. Rectangular cross-sections are also applied within the model for the finite element simulations (compare sub-figure b). b) Representative part of the tetrahedral structure to visualize the deletion of ligaments within the structure. Elements marked in blue are still active, elements marked in red are deactivated by reducing the stiffness to near-zero. Only vertical struts are deactivated, all nodes and all horizontal ligaments are still active.

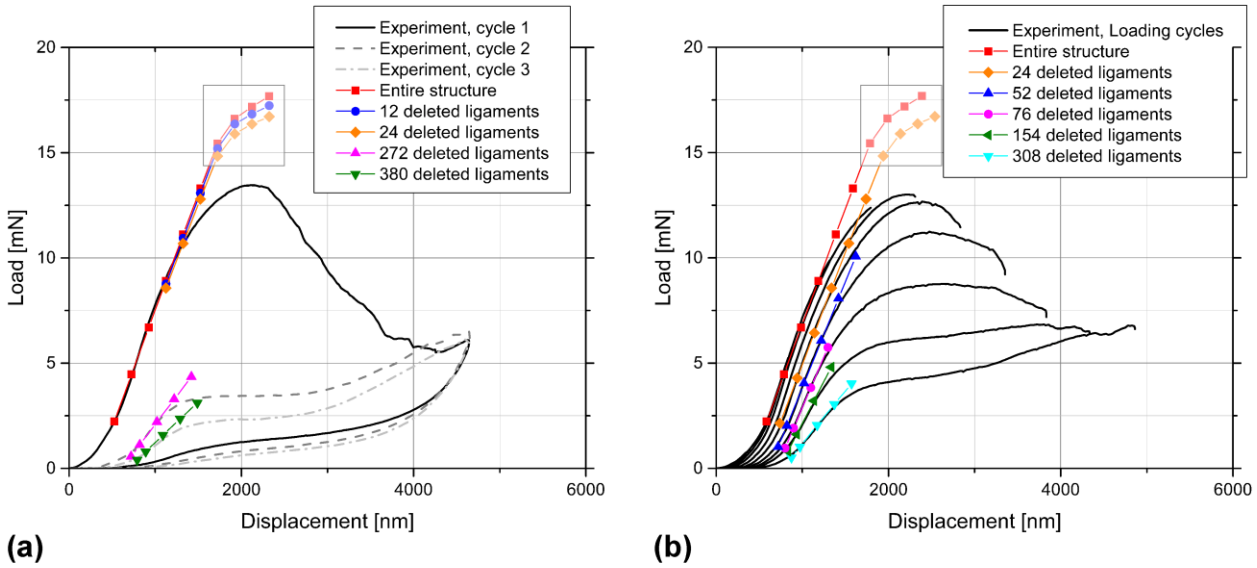

Figure S.9: Comparison of experimentally measured load-displacement curves for an annealed tetrahedral structure with vertical reaction forces calculated using finite element simulations. a) Comparison to first three cycles of cyclic loading to a maximum displacement of 5 µm, b) comparison to loading portions of progressive cyclic loading in steps of 500 nm to a maximum displacement of 5 µm. Due to symmetry reasons, only one half of the tetrahedral structure was simulated, however, the number of deleted ligaments stated in the legends of the graphs corresponds to the whole tetrahedral structure. The displacement values of the FE simulations are shifted horizontally to the corresponding experimentally measured curves, to account for misalignment and remaining strain values. The deviation from linear-elastic behavior within the FE simulations can only be attributed to geometrical nonlinearities due to the applied linear-elastic material behavior. To mark these values (displacement >1700 nm), they are overlaid with a shaded area.

Table S.4: Calculated solid material fractions and corresponding density values of all tested microlattices. Material fractions and density values are estimated using CAD models of a single unit cell of the individual structure. Additionally, the nominal maximum strain corresponding to the maximum displacement of 5 µm during compression testing is given for all structures.

	Processing	Solid material fraction [%]	Polymer fraction of solid material [%]	Al_2O_3 fraction of solid material [%]	Density [kg/m³]	Nominal maximum strain during compression testing [%]
Honeycomb	As-written	25.2	100	0	323	50
Hexagonal structure	As-written	9.6	100	0	123	25
Cubic structure	As-written	13.4	100	0	172	25
Tetrahedral structure	As-written	15.8	100	0	202	29
Tetrahedral structure	200°C/15 min	15.8	100	0	202	29
Tetrahedral structure	10 nm Al_2O_3 coating	21.3	96.4	3.6	285	29
Tetrahedral structure	100 nm Al_2O_3 coating	28.3	72.6	27.4	488	29

Video S.1: *In-situ* compression test of an annealed tetrahedral structure under cyclic loading to a maximum displacement of 5 µm for 20 cycles (shown at 10x speed). Most fracture events appear during the first loading cycle, however, further fracture events during following cycles are also visible. Strong recovery upon unloading can be observed, even after 20 loading cycles.

Video S.2: *In-situ* compression test of an as-written hexagonal structure to one loading cycle to a maximum displacement of 5 µm (shown at 5x speed). The structure is very prone to global and local buckling, followed by node fracture. Nevertheless, pronounced recovery upon unloading can be observed.

Video S.3: *In-situ* compression test of an as-written cubic structure to one loading cycle to a maximum displacement of 5 µm (shown at 5x speed). Buckling of the structure and the ligaments is visible during loading, followed by node fracture. Pronounced recovery upon unloading can be observed.

Video S.4: *In-situ* compression test of an as-written tetrahedral structure under cyclic loading to a maximum displacement of 5 µm (shown at 10x speed). Buckling of the structure and the ligaments is visible during loading and only a limited number of fractured nodes. Pronounced recovery upon unloading can be observed, however, the visible remaining stain is higher in comparison to the annealed tetrahedral structure (compare **Video S.1**).

Video S.5: *In-situ* compression test of a tetrahedral structure with 10 nm alumina coating to one loading cycle to a maximum displacement of 5 µm (shown at 5x speed). Catastrophic fracture of the structure can be observed and nearly no recovery upon unloading.